Supporting Information for "Survey of Thermal Plasma Ions in Saturn's Magnetosphere Utilizing Forward Models"

R. J. Wilson[1], F. Bagenal[1], A. M. Persoon[2]

[1]Laboratory for Atmospheric and Space Physics, University of Colorado Boulder, Boulder, Colorado, USA

[2]Department of Physics and Astronomy, University of Iowa, Iowa City, Iowa, USA.

Contents

Additional Supporting Information (Files uploaded separately)

1. 2017JA024117-ds01.csv: The file described in 'Data set S1: The LASP forward model fit parameters (both good and bad)

Corresponding author: R. J. Wilson, `rob.wilson@lasp.colorado.edu`

1 Introduction

The following pages contain supplementary material to the main article. Some is on specific methods and calibrations, others are figures to verify comments made in the main text.

The main text had many figures that binned the LASP data, plotted in a variety of ways. The bins were medians (50^{th} percentile) with lower and upper error bars of the 25^{th} and 75^{th} percentile. Tables for the binned 9 free parameters are provided in this document, with a table for each of three percentile groups for clarity. The local time binning values, and temperature anisotropies, are not quoted here, but you may use Data Set S1 to bin in any way required.

2 Saturn deSpun Sun (SSS) frame

The co-ordinate system used in this study and for the fitted velocity vectors is Saturn de-Spun-Sun (SSS) where $+z$ is the Saturn spin axis, $+y$ is defined as the cross product of the $+z$ with the Saturn-to-Sun vector, and $+x$ is defined as the cross product of $+y$ with $+z$. This is exactly equivalent to the co-ordinate system used in Thomsen2010 and referred to there as SZS, where $+x$ is 12 Hrs local time, and $+y$ is 18 Hrs local time. It is also the equivalent of the Juno missions JUNO_JSS frame, except with Saturn rather than Jupiter.

This is shown in figure 1, note that the sun lies in the Z-X plane, but is not necessarily at +X.

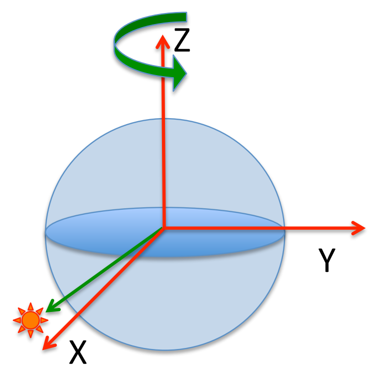

Figure 1. The Saturn de-Spun Sun system

This system has the Z-axis aligned with Saturn's spin axis but does not spin with the planet.

R_{SS} = unit vector of Saturn to Sun

$Z = S_{\Omega}$ = unit vector of Saturn's spin axis

$Y = Z \times R_{SS}$

$X = Y \times Z$

An alternative to Cartesian [X,Y,Z] coordinates, the SSS system can be expressed in radial distance, latitude and local time [R, Lat, LT],

$R = \sqrt{X^2 + Y^2 + Z^2}$

$Lat = arcsin(Z/R) * 180/\pi$, units of degrees

$LT = [(arctan(Y, X) + \pi) * 12/\pi]$ MOD 24, units of hours,

where arctan is the four quadrant inverse tangent of y and x. The MOD 24 is to keep LT in the range 0-24, and not -12 to +12.

3 Forward Model Fitting

3.1 The Forward Model

Equation 1 gives the equation that is minimized in order to find the best fit parameters, where $Cost$ is a χ_r^2 value if there are no penalties.

$$Cost = \frac{1}{num - \nu} \sum_{i=1}^{num} \frac{\left(O_i - B_i - S_i[\vec{P}]\right)^2}{\sigma_i^2} + 10^6 Penalty \tag{1}$$

where num is the number of data points to be fitted, ν is the number of free parameters ($\nu = 9$ for this study), O_i is the observed data from the SNG records (each energy step of each anode of each azimuth) and B_i is the background as calculated in the main text from the observed data. Since both observed and background values are from SNG data, they each have a combined uncertainty, σ_i. Assuming Poisson statistics and standard propagation of errors (while checking that $\sigma_i \neq 0$, as that causes infinities and code crashes) gives the equation for σ_i^2:

$$\sigma_i^2 = \begin{cases} \sigma_{O_i}^2 + \sigma_{B_i}^2 & \text{, if } \sigma_{O_i}^2 + \sigma_{B_i}^2 > 0 \\ 1 & \text{, if } \sigma_{O_i}^2 + \sigma_{B_i}^2 = 0 \end{cases} \tag{2}$$

The $S_i[\vec{P}]$ term is the simulated forward model count for element i when the free parameter vector $\vec{P}$ is applied to the model. In our case, $\vec{P} = [V_r, V_\theta, V_\phi, n_{W^+}, T_{\perp W^+}, T_{\parallel W^+}, n_{H^+}, T_{\perp H^+}, T_{\parallel H^+}]$. The model uses $\vec{P}$ to calculate an anisotropic Maxwellian distribution for both ions, moving at the same speed, then uses SNG calibrations (geometric factors and efficiencies) as well as applying instrument effects (such as cross talk) to simulate how many counts should be observed (see calibration section 3.2).

The $Penalty$ term is a value chosen to encourage the minimization code not to waste time doing unphysical fits. For this to work, $Penalty > 1$ always, and should be multiplied by a large term, hence 10^6 was used in equation 1, as all good CAPS fits in this study had $Cost$ less than 10^3. The penalty function is scaled rather than just being a constant. For instance, if a negative density was tried (would work mathematically in the equation, but is not physical), then a density of -1 is better than a density of -10. Both are bad, but this approach encourages the minimizing to work towards a less worse situation, then hopefully correct itself.

Penalties take several forms. Some are to remove unphysical situations, such as negative densities or temperatures ($Negative\_Cases$). Some are to keep the parameter space explored within defined upper and lower limits per free parameter ($Lower\_Lim\_Cases$ & $Upper\_Lim\_Cases$), avoiding wasting cpu time. Others place upper and lower limits on temperature anisotropies that are functions of multiple free parameters. And others look for best fits that match features of the data. The final $Cost$ equation begins to get very large, and is shown here, with the $Negative\_Cases$, $Lower\_Lim\_Cases$ & $Upper\_Lim\_Cases$ broken out to separate equations for reasons of space and clarity, but provide the actual upper and lower limits used for the LANL dataset fits.

$$Cost = \frac{1}{num - \nu} \sum_{i=1}^{num} \frac{\left(O_i - B_i - S_i[\vec{P}]\right)^2}{\sigma_i^2} + \begin{cases} Negative\_Cases & \\ Lower\_Lim\_Cases & \\ Upper\_Lim\_Cases & \\ & \\ 10^6 \left(1 + T_{\perp W+}/T_{\parallel W+}\right) & \text{, if } T_{\perp W+}/T_{\parallel W+} > 20 \\ 10^6 \left(1 + T_{\perp H+}/T_{\parallel H+}\right) & \text{, if } T_{\perp H+}/T_{\parallel H+} > 20 \\ 10^6 \left(1 + T_{\parallel W+}/T_{\perp W+}\right) & \text{, if } T_{\perp W+}/T_{\parallel W+} < 0.5 \\ 10^6 \left(1 + T_{\parallel H+}/T_{\perp H+}\right) & \text{, if } T_{\perp H+}/T_{\parallel H+} < 0.5 \\ 10^6 \left(1 + (2 - MaxS_{W+})\right) & \text{, if } MaxS_{W+} < 2 \text{ counts} \\ 10^6 \left(1 + (2 - MaxS_{H+})\right) & \text{, if } MaxS_{H+} < 2 \text{ counts} \\ 10^6 \left(1 + |MaxAnC - MaxAnS|\right) & \text{, if } |MaxAnC - MaxAnS| > 1 \\ 10^6 \left(1 + |MaxEstC - MaxEstS|\right) & \text{, if } |MaxEstC - MaxEstS| > 4 \\ 10^6 \left(1 + MaxEvS_{H+} - MaxEvS_{W+}\right) & \text{, if } MaxEvS_{H+} >= MaxEvS_{W+} \\ & \\ 0 & \text{, otherwise} \end{cases} \tag{3}$$

$$Negative\_Cases = \left\{ 10^6 \left(1 - \xi\right) \quad \text{, if } \xi < 0 \text{ where } \xi \in \left\{ n_{W+}, T_{\perp W+}, T_{\parallel W+}, n_{H+}, T_{\perp H+}, T_{\parallel H+} \right\} \right. \tag{4}$$

$$Lower\_Lim\_Cases = \begin{cases} 10^6 \left(1 + |-500 - V_r|\right) & \text{, if } V_r < -500 \text{ km/s} \\ 10^6 \left(1 + |-500 - V_\theta|\right) & \text{, if } V_\theta < -500 \text{ km/s} \\ 10^6 \left(1 + |-500 - V_\phi|\right) & \text{, if } V_\phi < -500 \text{ km/s} \\ 10^6 \left(1 + |0.001 - n_{W+}|\right) & \text{, if } n_{W+} < 0.001 \text{ cm}^{-3} \\ 10^6 \left(1 + |0.001 - T_{\perp W+}|\right) & \text{, if } T_{\perp W+} < 0.001 \text{ eV} \\ 10^6 \left(1 + |0.001 - T_{\parallel W+}|\right) & \text{, if } T_{\parallel W+} < 0.001 \text{ eV} \\ 10^6 \left(1 + |0.001 - n_{H+}|\right) & \text{, if } n_{H+} < 0.001 \text{ cm}^{-3} \\ 10^6 \left(1 + |0.001 - T_{\perp H+}|\right) & \text{, if } T_{\perp H+} < 0.001 \text{ eV} \\ 10^6 \left(1 + |0.001 - T_{\parallel H+}|\right) & \text{, if } T_{\parallel H+} < 0.001 \text{ eV} \end{cases} \tag{5}$$

$$Upper\_Lim\_Cases = \begin{cases} 10^6 \left(1 + |500 - V_r|\right) & \text{, if } V_r > 500 \text{ km/s} \\ 10^6 \left(1 + |500 - V_\theta|\right) & \text{, if } V_\theta > 500 \text{ km/s} \\ 10^6 \left(1 + |3V_{Corot.} - V_\phi|\right) & \text{, if } V_\phi > 3V_{Corot.} \\ 10^6 \left(1 + |1500 - V_\phi|\right) & \text{, if } V_\phi > 1500 \\ 10^6 \left(1 + |100 - n_{W+}|\right) & \text{, if } n_{W+} > 100 \text{ cm}^{-3} \text{ and if } R \leq 15R_S \\ 10^6 \left(1 + |10 - n_{W+}|\right) & \text{, if } n_{W+} > 10 \text{ cm}^{-3} \text{ and if } R > 15R_S \\ 10^6 \left(1 + |10^5 - T_{\perp W+}|\right) & \text{, if } T_{\perp W+} > 10^5 \text{ eV} \\ 10^6 \left(1 + |10^5 - T_{\parallel W+}|\right) & \text{, if } T_{\parallel W+} > 10^5 \text{ eV} \\ 10^6 \left(1 + |100 - n_{H+}|\right) & \text{, if } n_{H+} > 100 \text{ cm}^{-3} \text{ and if } R \leq 15R_S \\ 10^6 \left(1 + |10 - n_{H+}|\right) & \text{, if } n_{H+} > 10 \text{ cm}^{-3} \text{ and if } R > 15R_S \\ 10^6 \left(1 + |10^5 - T_{\perp H+}|\right) & \text{, if } T_{\perp H+} > 10^5 \text{ eV} \\ 10^6 \left(1 + |10^5 - T_{\parallel H+}|\right) & \text{, if } T_{\parallel H+} > 10^5 \text{ eV} \end{cases} \tag{6}$$

Note that in the lower limits defined above, densities and temperatures can not be negative, hence the $Negative\_Cases$ are redundant, but kept in for safety.

Equation 3 clearly shows the enforced anisotropy limits where $0.5 < T_\perp/T_\parallel < 20$.

The $1+(2-MaxS)$ terms are to ensure that all ion species are fitted, where $MaxS$ is the MAXimum Simulated count for any index i. If less than 2 counts are simulated for a given ion species, then that ion species essentially isn't present and you should not be trying to fit it.

The $1+|MaxAnC-MaxAnS|$ term is to enforce the simulated anode with the maximum counts to be within at least 1 anode of the observed anode with the most counts, where $MaxAnC$ is the Maximum Count Anode, and $MaxAnS$ is the Maximum Simulated count Anode. It was found that enforcing the simulated counts to match the maximum anode perfectly did not always work and it is better to allow a little wiggle room.

Similarly, The $1 + |MaxEstC - MaxEstS|$ term ensures that the Energy Step that had the peak simulated counts ($MaxEstS$) matches the energy step with the peak observed Counts ($MaxEstC$), at least to within 4 energy steps. As before, this requires some wiggle room and being within 4 energy steps was found to be a good compromise.

The final term is the $1+MaxEvS_{H+}-MaxEvS_{W+}$ one, that ensures that the heavier ion species has a distribution that peaks in counts at a higher energy step (in eV) than the lighter ion species' distribution (where $MaxEvS$ is the Maximum eV Step).

When the free parameter vector $\vec{P}$ is in the general vicinity of the best fit solution, no penalties should be hit and the equation simplifies to a reduced Chi square.

However, when a fit had finished, one should always check that none of the best fit values are on (or even near) one of the upper or lower limits (including the anisotropy one), as shown in the main article text. The above Cost function equation can exit right on a limit, therefore this must be checked for. If uncertainties are calculated, then when exactly on a limit the uncertainties go insanely tiny (as in chi-square space, sampling one side of the best fit gives a slightly bigger Cost, but sampling the forbidden area results in a cost of $\geq 10^6$, creating an extremely step curvature, and as such a ridiculously tiny uncertainty. General rule, if the uncertainty is under 1%, do not believe it was a good fit. Exceptions for velocity components which may have values near zero, and so a percentage is no longer a useful measure. If your code keeps hitting a limit, alter your limits until that is no longer a problem.

For the LASP dataset, as shown in the above equations, the limits were:

1. Each velocity component had a minimum limit of -500 km/s and a maximum limit of +500 km/s, with the exception of V_ϕ which had a maximum limit of the smaller of 1500 km/s or $3V_{Corot.}$ (where $V_{Corot.}$ is the rigid corotation velocity at Cassini's current location). (Three times rigid corotation was excessive but to allow for the possibility of super-corotation, not that any was found.)
2. Temperatures have a lower limit of 0.001 eV and an upper limit of 10000 eV.

3. The density lower limit is always 0.001 cm^{-3}, while the upper limit is 100 cm^{-3} when Cassini is within 15 R_S, otherwise the density upper limit is 10 cm^{-3}.

Another item to be careful of is missing data, either in the raw data itself, or introduced in the pre-/post-pruning process. Any element O_i that is equal to the MISSING_CONSTANT (fill) value should be excluded from equation 3, and num reduced accordingly. If $num < \nu$ then the interval can not be fit.

There is also the issue of count quantization in spacecraft data to account for. Generally the onboard instrument is literally counting counts, for SNG data this in on a 16-bit counter. However there is not enough bandwidth to return all these 2-byte numbers, so they are lossy compressed to a 1-byte value and transmitted. This is discussed in the CAPS Users Guide (section 7.7 “Count quantization for SNG, ION, ELS and TOF”) which includes a table of all 256 quantized values that SNG Level 2 counts per accumulation data can have. For instance, the 1-byte value 100 represents for SNG data 203 counts (as shown in the table in the Users guide). The 1-byte value 101 represents 209 counts. Therefore the 1-byte value 100 really represents the range 203-208 counts, the upper range being 1 count less than the next 1-byte's value decimal equivalent.

For normal use, everyone uses the values that come out of the Level 2 data files, which are the lower edge of the range of each quantized bin. For CAPS SNG community convention, we do the same, so that O_i and B_i are those values. The uncertainties of those values are found assuming Poisson statistics, hence are the square root if the counts, which is underestimating the true uncertainty of the range. To somewhat address this, for the uncertainty values we use the square root of the upper limits of the quantized values. e.g. for the earlier example, the quantized value represented by the 1-byte value 100 is now $203 \pm \sqrt{208}$ (e.g. $lower_i \pm \sqrt{upper_i}$). This is done for both σ_{O_i} and σ_{B_i}.

[Technically we should probably have used

$$(upper_i + lower_i)/2 \pm \sqrt{(upper_i + lower_i)/2 + ((upper_i - lower_i)/2)^2)}$$

but it did not seem to make a significant difference. For Juno's JADE data analysis a more complicated approach such as this is used, based on the lessons here of Cassini CAPS analysis.]

Finally, even with all these checks, constraints and limits, there is no guarantee that the final fit is good. This is finding the best mathematical fit, which may not be the best physical fit, and the fit may have ignored many data points (or for example, put the simulated proton peak in the observed water group peak, pushing the simulated water group ions to the high energy tail and thus producing an unrealistically high velocity). This may be due to poor quality data to fit to, or maybe the minimization code in use found a local, rather than the global, minimum. Re-running the fits multiple times to find the best of the best-fits is most likely to ensure you find the global minimum. The LASP dataset has fits that were re-run many, many times to give it the best chance, but it is certain that some bad fits got through. The only way to know for certain is to check all fits by eye, which is impractical for large surveys. Be cautious.

3.2 Calibrations Used For The Forward Model of This Study

The calibrations values were taken from the CAPS Users Guide (section 8.3):

Wilson, R. J., et al. (2012), PDS User's Guide for Cassini Plasma Spectrometer (CAPS), Planetary Data System. [Available at http://ppi.pds.nasa.gov/.]

For the two ion species used in the study, SNG efficiencies for H^+ and OH^+ (for W^+), both with the c term as 0.85, were used.

[By contrast, Wilson2008 & Thomsen2010 had used the scalar 0.266 efficiency value for all, rather than any ion species dependent or energy dependent values, as those were not available at the time.]

The anode cross talk matrix provided in the CAPS Users Guide was included in the simulated counts before matching them to the observed data.

The operational voltage of CAPS IMS was fixed for nearly the entire mission, except the last few days of CAPS. At 2012-05-16T03:02:34 the microchannel plate's operational voltage was raised for science operations for the first time and the final few days, presumingly because the SNG efficiency was starting to decrease from the expected value, and the increase should counter that. This only affected the last 346 'good' (records with JGR=1 in data set S1) LASP records and in principle increasing the SNG efficiencies back to where it should be.

However, at time of writing there is no official document on how the microchannel plate's gain (and therefore SNG efficiency) varied over the mission, and so the calibrations provided in the Users Guide are used.

3.3 Pre-pruning

The main article text explains how suitable half-actuation periods of SNG data are found (one actuator extreme to the other, removing unsuitable ones).

This gave 36,588 half-actuation periods to forward model fit. Each period needs a unit magnetic field vector assigned to it, using the 1-minute averaged data available on the PDS. It is assumed that the plasma environment (and therefore magnetic field vector) is stable during the interval, so the magnetic field value closest to the center time of the period is used. If there is plasma data but no corresponding magnetometer data, the period is rejected. For look direction angles of CAPS IMS, the center times of each SNG record are used. e.g. if the SNG data is at 32 second resolution per record, the actuator moved up to 32° during that time (less if near an actuation edge, or turned around at an edge), then the look direction 16 seconds from the start of that record is used for that record. This involves interpolating the actuator angles and orientation information given in the ACT (actuator) and ANC (ancillary) files present in the CAPS PDS volume.

A background must be calculated for each SNG anode each record, which is carried out by assuming that for each energy sweep, 95% of the energy steps are above background. However we exclude the top few energy steps as usual (see the CAPS Users Guide), plus energy step 4, so only considered energy steps 5 to 63 but also removing any energy step that has a PDS MISSING_CONSTANT value (i.e. a fill value when counts for that energy step are unknown). The energy steps are re-ordering in to increasing measured counts, and the value of the energy step that falls at 5% of the number of remaining energy steps is considered the background value. For the usual case of no MISSING_CONSTANT values, there are 59 energy steps in consideration, which are re-ordered by increasing values, and the 5% step is the one at the second index ($= floor(59 * 0.05) = 2$) of the re-ordered data. Therefore just sorting the 59 values and taking the 2^{nd} index of the sorted values provides the background for each anode per energy sweep. That background then applies for all energy steps for that anode and azimuth.

As stated in the CAPS Users Guide, energy steps 1-3 of SNG data are considered useless, so those are ignored within the forward model fit, which we do by setting them to the MISSING_CONSTANT value.

The remaining data are valid (and now has a background value per anode per azimuth), but not all of that data is useful in the fitting procedure. For instance, any look direction perpendicular to the ion flow direction will have no signal, only noise. Including such extraneous data points only serve to make a worse fit (and thus increase the uncertainty on the fitted parameters, see Appendix A of *Wilson et al.,* (2013), where this is discussed in depth) and also take extra cpu time. To further pre-prune the data we exclude extraneous data by setting them to the MISSING_CONSTANT value, and coding the minimization code to ignore such values from the fit. Extraneous data is found by two rules, followed after converting the counts per accumulation to counts per second (after background removal) and identifying the anode/energy-step with the greatest counts/second signal, which is the peak-count look direction. The necessity to convert to counts per second is because the telemetry mode (and hence accumulation time per record) may change during an interval. The two rules to locate extraneous data are:

1. Any data element with a look direction that is more than 65° away (in any direction) from the peak-count look direction is removed.
2. Any data element that has a counts per second value smaller than $1/50^{th}$ of the peak-count look direction signal is removed.

This leaves data with plenty of signal in multiple directions, with a FOV reduced from the original $\approx 2\pi$, that is faster to analyze and also provides lower uncertainties to the fitted parameters.

If a similar technique is used for other mission's data, the angular acceptance and count ratio would need to be carefully chosen - blindly using those stated here for CAPS SNGs would be unlikely to yield the best results.

[By comparison, for Galileo PLS data analysis [*Bagenal et al.*, (2016)], a similar technique was used but with different values. The look direction acceptance was split in to two rules, the first different to that used for this study. Data from the peak-count anode and the nearest immediate neighbor anodes each side were kept, other anodes were ignored (if the peak-count anode was at an end anode (PLS anode 1 or 7) then only neighbors on one side were considered, and if the immediate nearest neighbour anode was nothing but MISSING_CONSTANT values (missing the record, as happened frequently due to how the data products were decimated after Galileo's main antenna failed to deploy), then the next nearest non-missing anode was used). Then the angular acceptance was adjust so that for high rate PLS data (8 azimuths per spin) the angular acceptance was 67.5°, or 135° for other rates (4 azimuths per spin). For the count filter, the energy step of the peak counts direction was found, all energy steps from 8 below to 8 above that was kept, others removed. This was because in non-high-rate modes only every 3^{rd} of 4^{th} energy step was populated due to the limited telemetry Galileo had.]

References

Bagenal, F., R. J. Wilson, S. Siler, W. R. Paterson, and W. S. Kurth (2016), Survey of Galileo plasma observations in Jupiter's plasma sheet, J. Geophys. Res. Planets, 121, 871894, doi:10.1002/2016JE005009.

Wilson, R. J., et al. (2012), PDS User's Guide for Cassini Plasma Spectrometer (CAPS), Planetary Data System. [Available at http://ppi.pds.nasa.gov/.]

Wilson, R. J., F. Bagenal, P. A. Delamere, M. Desroche, B. L. Fleshman, and V. Dols (2013), Evidence from radial velocity measurements of a global electric field in Saturn's inner magnetosphere, J. Geophys. Res. Space Physics, 118, 21222132, doi:10.1002/jgra.50251.

4 Figures

4.1 Petal Plots of LASP Data in Different Co-ordinate Systems

Figure 2 and 3 show the 'good' LASP moments, one free parameter at a time, on petal plots. Figure 2 is in a SLS3 co-ordinate system and only include LASP data from the SLS3 epoch of relevance to Cassini (2004 through to 2007T222). Figure 3 show the LASP data in Local time over the entire CAPS mission (2004-2012).

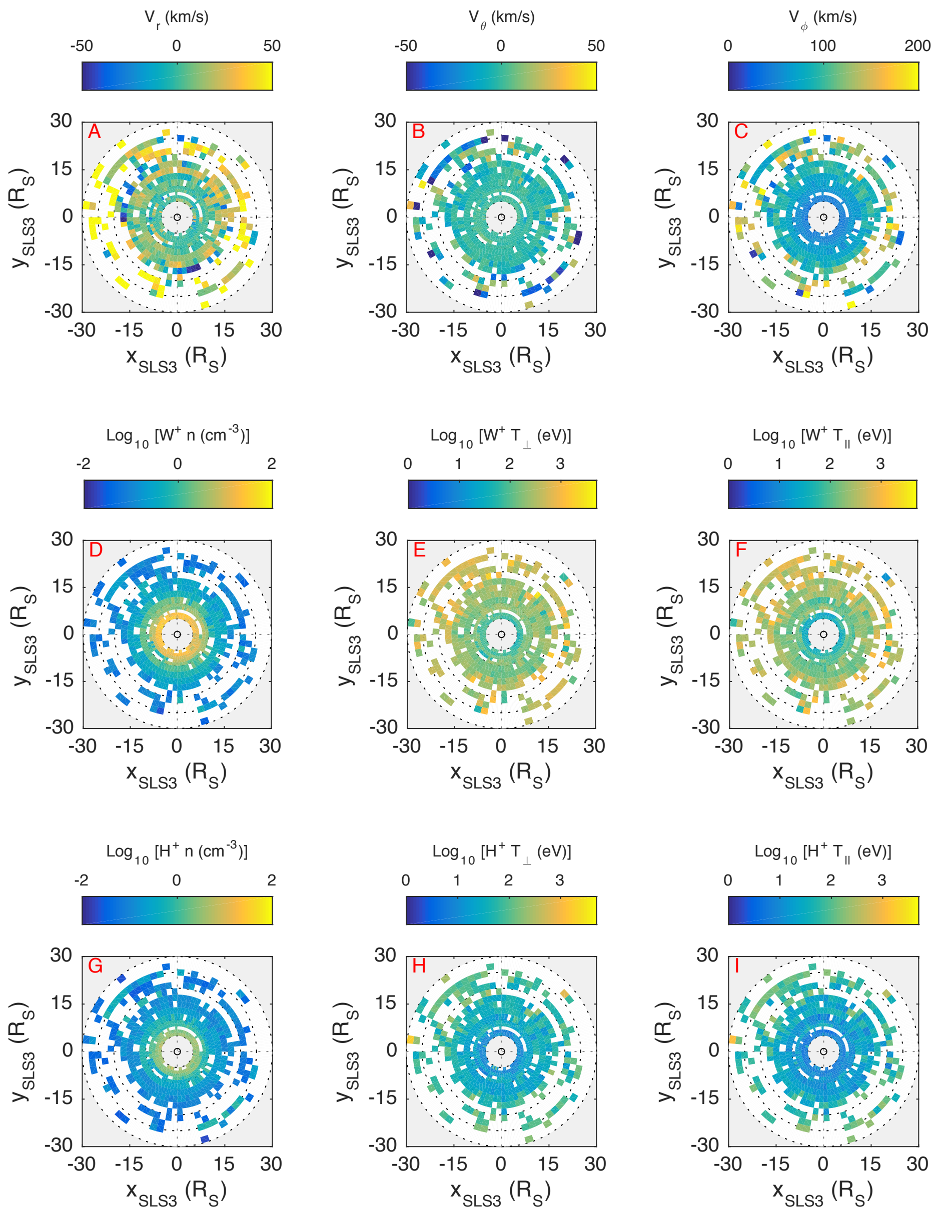

Figure 2. SLS3 Petal Plots of the 9 LASP fitted parameters, during the SLS3 epoch of 2004 to 2007T222 that had 2974 records. East Longitude co-ordinates would be such that +x = 0° and that +y = 90°.

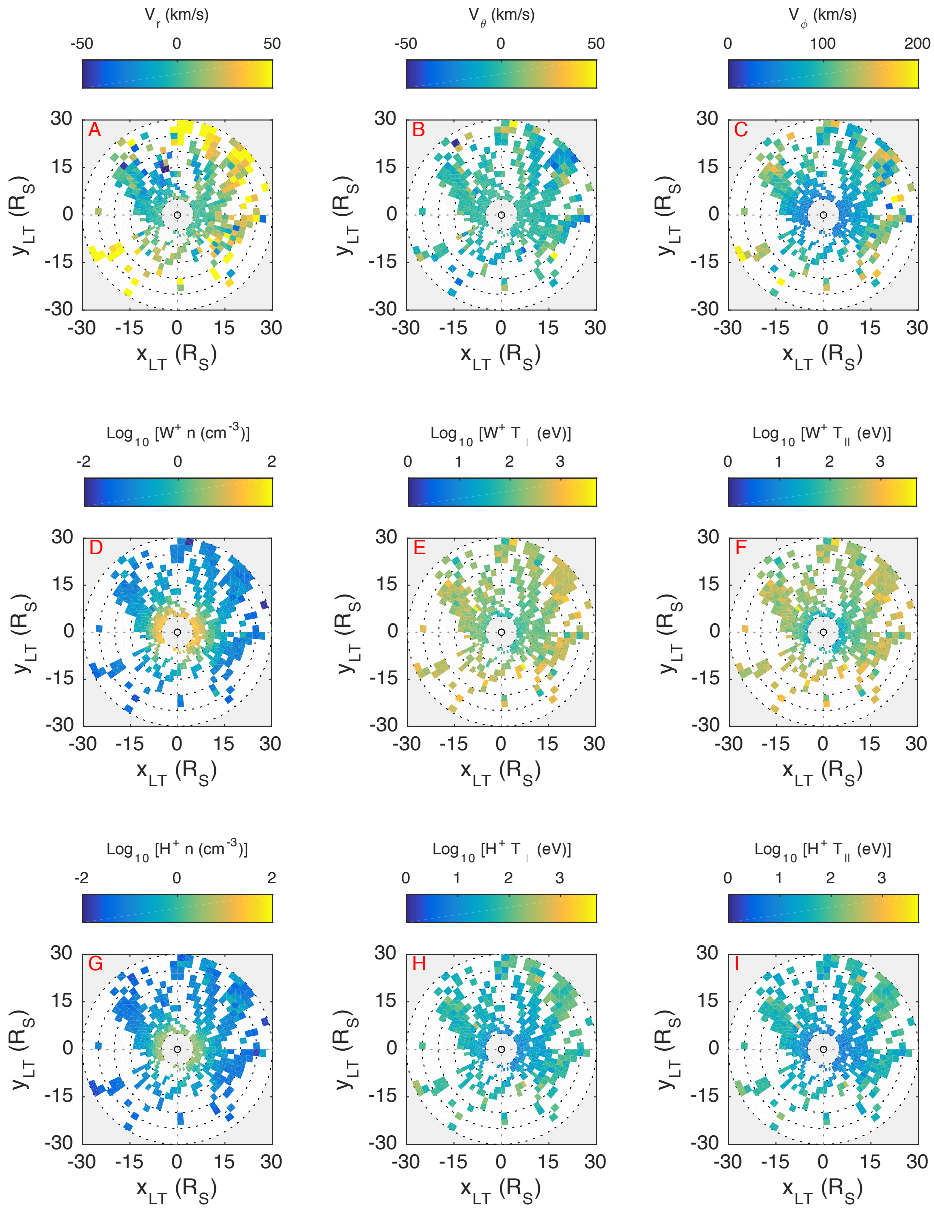

Figure 3. Local Time Petal Plots of the 9 LASP fitted parameters, during the entire CAPS mission of 2004 to 2012 that had 9736 records.

4.2 Raw Data That Was Confused For Evidence of Super-Corotation

Figures 4 and 5 consist of four panels taken from the fourth interval of the *Masters et al.* (2011) study that indicted super-corotation flow in the LANL dataset. Each panel is an energy-time spectrogram (averaged over all 8 SNG anodes), where energy is expressed in energy step number of 1-63 (1 is high, 63 is low eV), and the x-axis is UTC hours:minute, of the date given in the panel title. Each panel covers one half-actuation period as used in this study. The magenta curve overlaid on each plot is the actuator angle on an arbitrary linear scale to highlight when the actuator is at each extreme and when it's moving from one side to the other. Panels A, B and C are all cases where the plasma environment is changing faster than the instrument cadence of half-actuation periods, which invalidates the Forward Model and numerical moments approaches that both assume the plasma environment is stable during the interval.

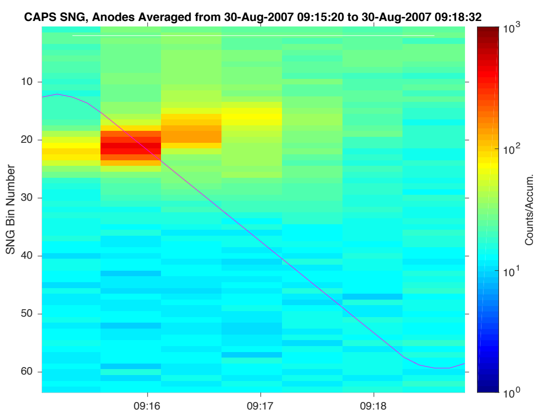

A

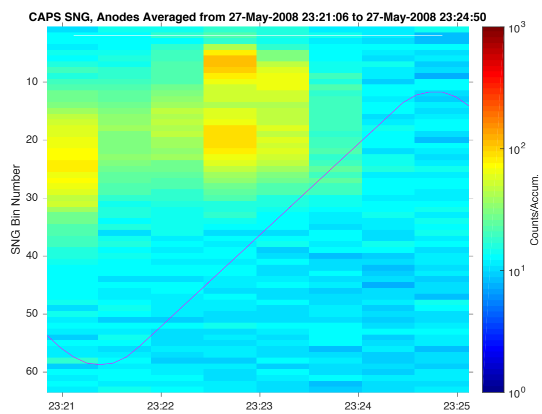

B

Figure 4. Examples #1 of half-actuation periods that are not suitable for fitting, but if used may suggest super-corotation velocites.

Panel A's second column has the most counts, peaking around energy step (bin) 20. However the neighboring columns 1 and 3 (and 4) show the peak counts at different energies, indicating that the plasma is moving to higher energies during this interval. Panel B nicely shows both a W^+ and H^+ distribution in the fourth column, which according to the actuator angle (magenta line) occurs during the middle of the actuator sweep. However there is a further bright distribution in the first column near the actuator extreme, indicating that the plasma has changed direction, as well as energy and differing number of significant ion species, during the interval. Panel D (figure 5) shows a similar case of the plasma environment changing, both in energy and also direction.

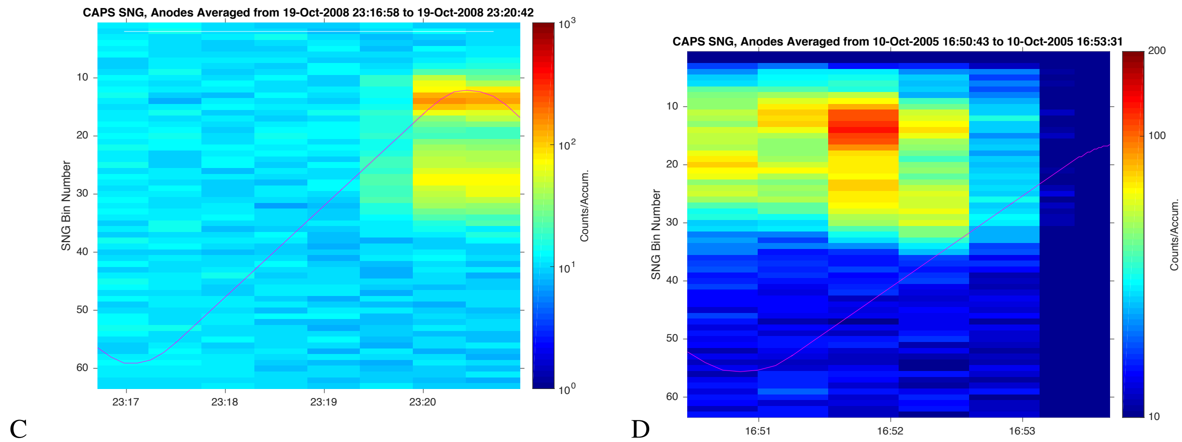

Figure 5. Examples #2 of half-actuation periods that are not suitable for fitting, but if used may suggest super-corotation velocites.

Panel C of figure 5 does not show a case where the plasma environment is changing, however still is unsuitable to be used to generate plasma parameters. The issue is that the peak counts are observed right at the edge of the actuator extreme. This likely means the true ion beam was just outside the field of view of the CAPS instrument, which was only able to measure the 'foot-hills' of the plasma distribution, and not the core of main distribution. Since the main core of the distribution is missed, the density can not be calculated as we do not know how 'high' in counts the distribution would have peaked at. For numerical moments, the first order moment is nV, and if n can not be found then V will be incorrect.

Unfortunately, all the intervals identified in numerical moments as super-corotating can be rejected as poor viewing (e.g. panel C) or as the plasma environment changing faster than our moments cadence.

The post-pruning filters of this study did a decent job of removing these intervals from our 'good' set, however the filters are not perfect. The top panel of figure 6 shows the LASP pre-pruned $V_\phi \pm \sigma_{V_\phi}$ data in green + symbols, with rigid-corotation shown in black. Of the 14 LASP intervals within the *Masters et al.* (2011) region, only 2 intervals passed the post-pruning, shown with green x symbols to make an Asterix. The bottom panel of the plot shows the water (blue) and proton (red) densities on a linear scale, with similar + and x marking to identify the pre/post-pruned intervals. It is clear the uncertainties of those two LASP fitted parameters are on the larger side. However, on closer inspection, two post-pruned 'good' records turned out to be cases where the plasma environment was changing, hence are not to be trusted.

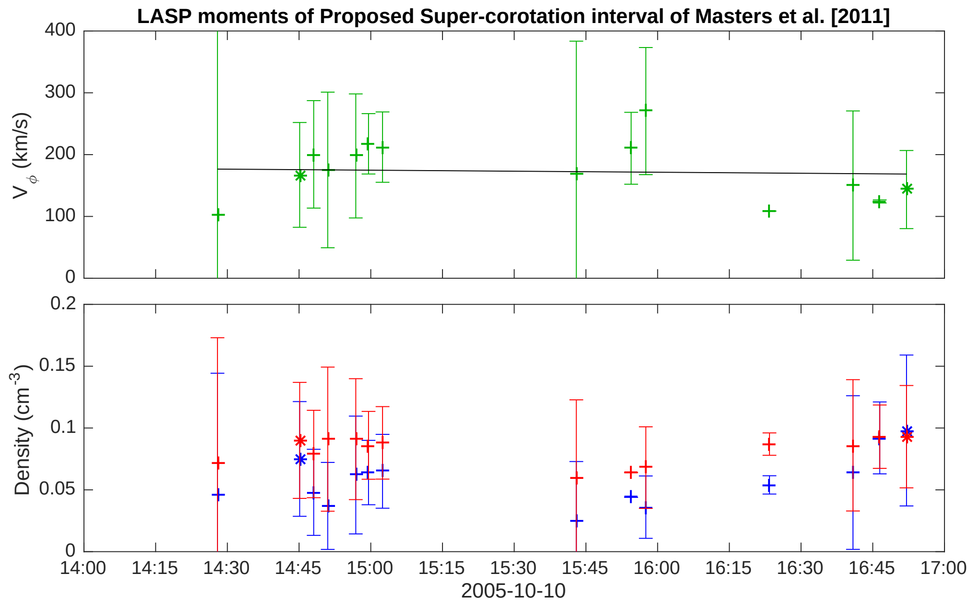

Figure 6. 2 'good' fits out of 14 potential ones that were all filtered as bad bad during the proposed Masters Super-corotation

The second one (about 16:50) that passed the post-pruning is shown in panel D of figure 5, where it is obvious the plasma environment is not stable.

Panel D should be a cautionary tale to all who use survey plasma parameters - just because your chosen code (be it forward modeling or numerical moments) provides an answer, it may not be physical. It is best to look for trends in parameter data, that neighboring points have similar values (so called persistence), and if so, then those values are likely trust worthy. But values that appear as outliers, or have neighbors that vary wildly, should be checked by returning to the raw plasma counts and seeing if the plasma environment was changing, or the field of view unsuitable.

References

Masters, A., M. F. Thomsen, S. V. Badman, C. S. Arridge, D. T. Young, A. J. Coates, and M. K. Dougherty (2011), Supercorotating return flow from reconnection in Saturn's magnetotail, Geophys. Res. Lett., 38, L03103, doi:10.1029/2010GL046149.

4.3 LASP vs. LANL Survey Comparisons

How do LASP and LANL profiles compare? Despite both datasets being survey data over the whole CAPS mission, they are often from different times with LANL moments having many more records, often in lower density regions than LASP moments sample (due to LASP requirement to have a distribution that peaks with >100 counts). This is highlighted in figure 7 where LASP densities have minimums about 0.1 cm^{-3}, while LANL densities reach 0.01 cm^{-3}, at least for the regions when there is near-coincident LASP and LANL data points (see figure caption). The left panel is a scatter plot of the respective total densities, with every 10th errorbar shown on the total LASP density to give a sense of scale. The right panel bins the LASP data using LANL total density ranges and shows the LASP median with errorbars of 25th and 75th percentiles (the binning is carried out in $\log_{10}$ space (-3 to 2), every 0.1 from -3 to 0, then every 0.05). LANL densities are generally greater then those of LASP to around the 0.55 cm^{-3} mark (roughly corresponds to $\approx$15 R_S), and in lower densities regions LASP densities are significantly greater than LANL's.

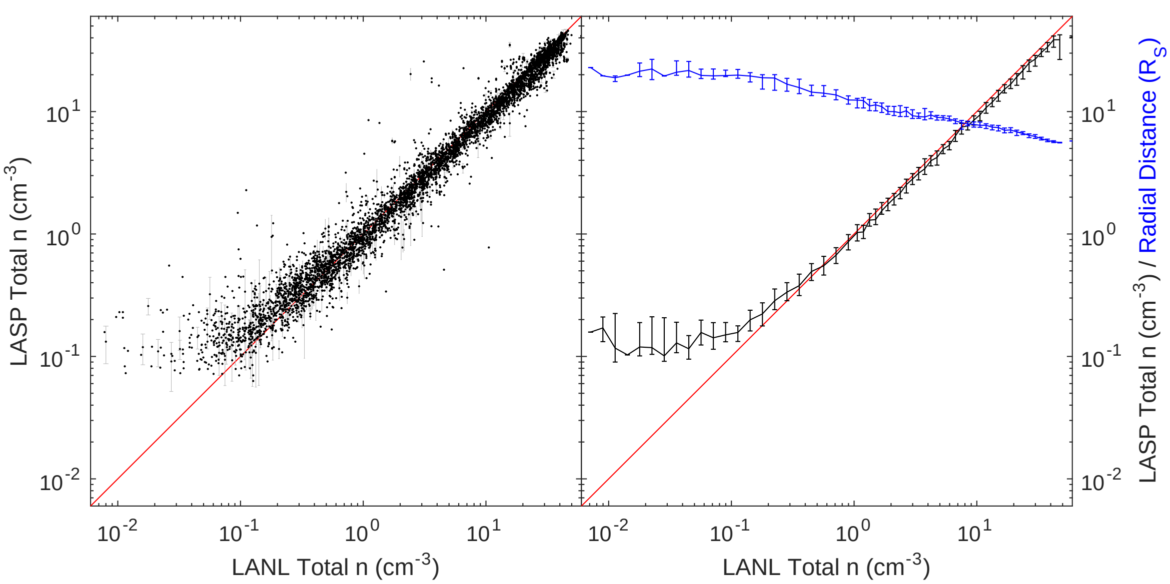

Figure 7. Comparing the LASP and LANL plasma densities. A comparison of total density is shown (n_{W^+} + n_{H^+} for LASP and n_{W^+} + $n_{H_2^+}$ + n_{H^+} for LANL) of 'good' data points for both datasets and only when the time elements are within 3 minutes of each other. That left 5,222 LASP matching intervals between the two datasets, shown here. There were 3,434 LANL matches (as LASP time cadence is about double that of LANL), hence some LANL points are used for multiple LASP times. The blue line shows the radial distance of each interval, binned in the same way. The straight red line is the 1:1 ratio line.

Figure 8 is a copy of the figure from the main article text that bins all data in each survey (9736 LASP records to 15958 LANL), while figure 9 is similar binning, when both LASP and LANL data are restricted to times that are no further than 10 minutes from each other. Figure 10 is the same again, restricted to times no further than 3 minutes from each other.

Since most of the intervals are within $15R_S$ there are relatively few intervals to compare with at larger distances. However it remains true that LANL densities are greater than LASP ones when $<\approx 9R_S$, and LANL densities are less than LASP ones when $>\approx 10R_S$. By only considering data points near to each other, the differences in density do get smaller. This reinforces the idea that a profile of density, for example, taken from the full LANL dataset will be different to a profile of density from the full LASP dataset, just because the sampling of the two datasets are not from the same locations.

So when using similar locations (figure 10) the density profiles do have a better match much than the 'all' data case of figure 8. Yet the temperatures, especially for H^+ remain very different. The numerical moments technique used for the LANL dataset will include contributions of the high energy tail rather than just the core, but the difference between LANL and the Maxwellian fits (no tail included) of LASP are thought to be too great for that to be the sole explanation.

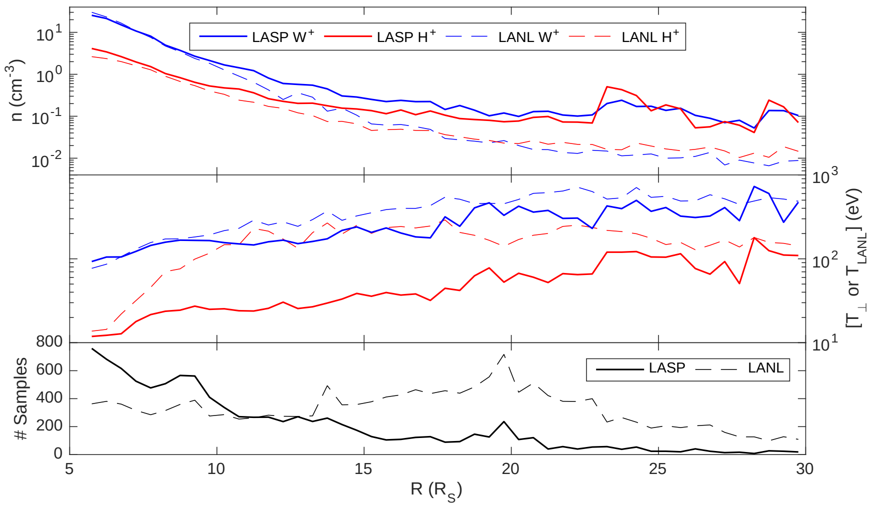

Figure 8. [Copied from main article] Comparing LASP (solid) and LANL (dashed) plasma parameters, medians of $0.5R_S$ bins. Top panel is density, middle panel is temperatures ($T_\perp$ for LASP, T for LANL), and bottom panel is the number of samples. Top two panels use the same legend. LANL data was filtered match LASP data location requirements (within 10° of equator, $5.5 < R_S < 30$).

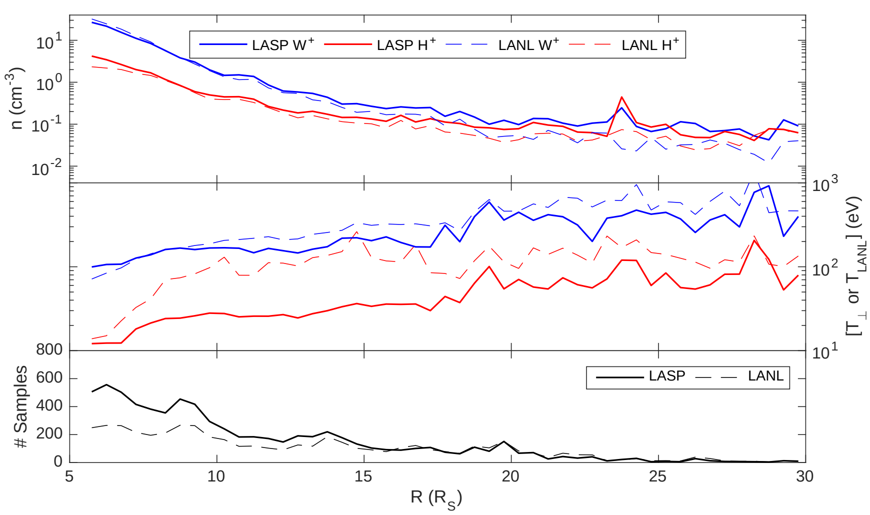

Figure 9. Same as Fig. 8 but using only LASP and LANL data that are from the same times (records used for binning must be within 10 mins of a record from the other data set (7144 LASP records to 4983 LANL).

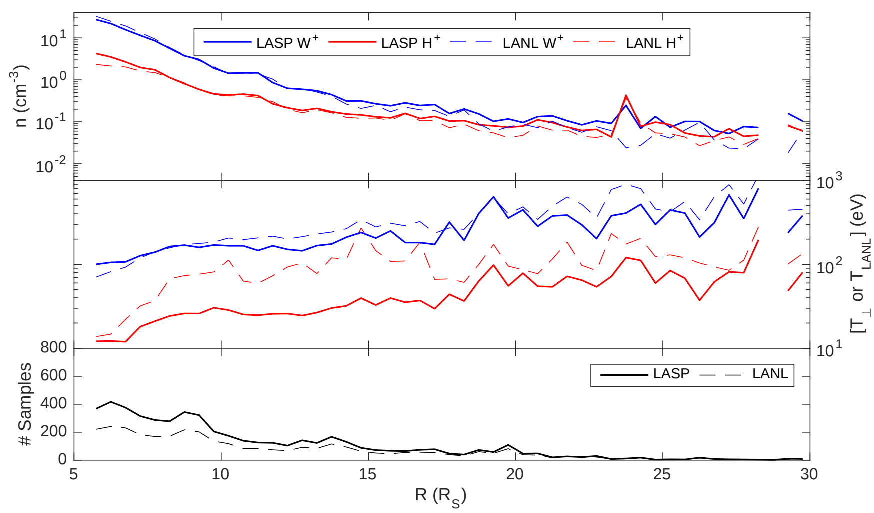

384 **Figure 10.** Same as Fig. 8 but using only LASP and LANL data that are from the same times (records used
385 for binning must be within 3 mins of a record from the other data set (5222 LASP records to 3434 LANL).

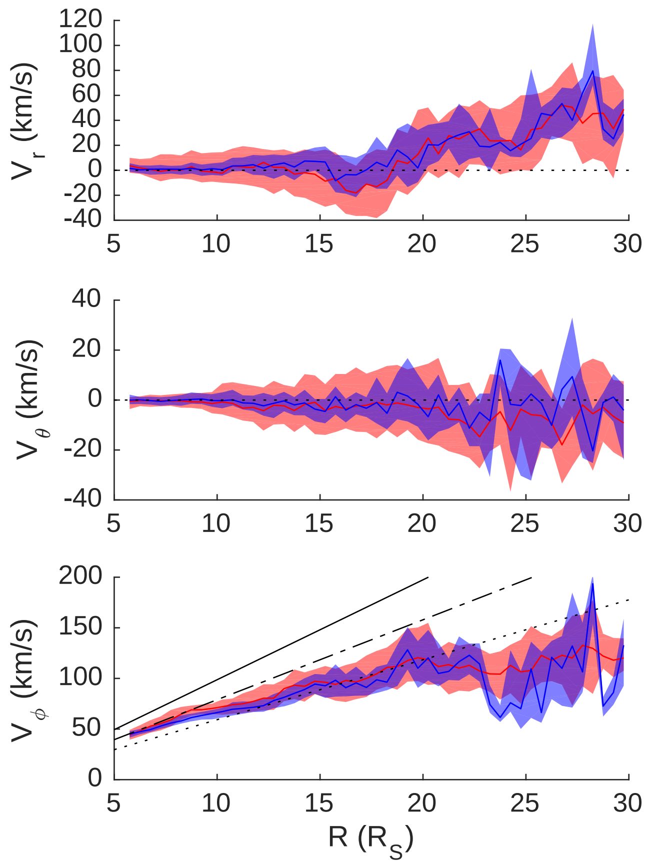

Figure 11. Binned Velocity profile comparisons of LASP (blue) and LANL data (red). Center lines are the medians, semi-transparent areas show the 25^{th} to 75^{th} percentile ranges. Horizontal line on top two plots are at zero, while the solid/dash-dot/dotted lines on the bottom panel are 100%/80%/60% corotation lines.

Figure 11 compares LASP and LANL velocity components, which are not too different. The 25^{th} to 75^{th} percentile ranges are generally smaller for the LASP dataset than LANLs.

4.4 Example LANL Moments Cases in Very Low Count Environments

The LANL survey includes low count regions that are too low to be used in the LASP survey. The LASP survey has a lower limit on how few counts are acceptable to do a forward model fit, simply because there needs to be enough counts over multiple energy steps, anodes and azimuth angles (actuator) that there is a recognizable shape that can be fit. Too few counts, or sporadic counts, result in just fitting a shape to noise, which has no physical meaning.

The LANL numerical moments includes regions where the maximum counts in an interval are as low as 27 counts. Figure 12 show two intervals, chosen as having the two lowest total densities of the LANL moments used for comparison in this study. Since the LANL moments only provide a start time, we assumed each interval was 15 A-cycles long (an upper estimate). As earlier, the magenta line indicates the actuator angles (seeing a full one-and-some actuation), while the white line marks telemetry mode.

These fits gave very low densities, the left side had [n_{W+}= 0.0010 cm^{-3}, $n_{H_2^+}$= 0.0013 cm^{-3}, n_{H+}= 0.0011 cm^{-3}], while the right side gave [n_{W+}= 0.0011 cm^{-3}, $n_{H_2^+}$= 0.0012 cm^{-3}, n_{H+}= 0.0013 cm^{-3}]. Since $n_{W+} \approx n_{H_2^+} \approx n_{H+}$ it may be inferred that this is a region of low count statistics, such that the numerical moments is essentially fitting noise.

The implication is that there is likely a point where observed counts are too low for the LANL numerical moments technique to provide valid moments, and such intervals should not be considered. Where low count statistics become an issue is out of the scope of this study.

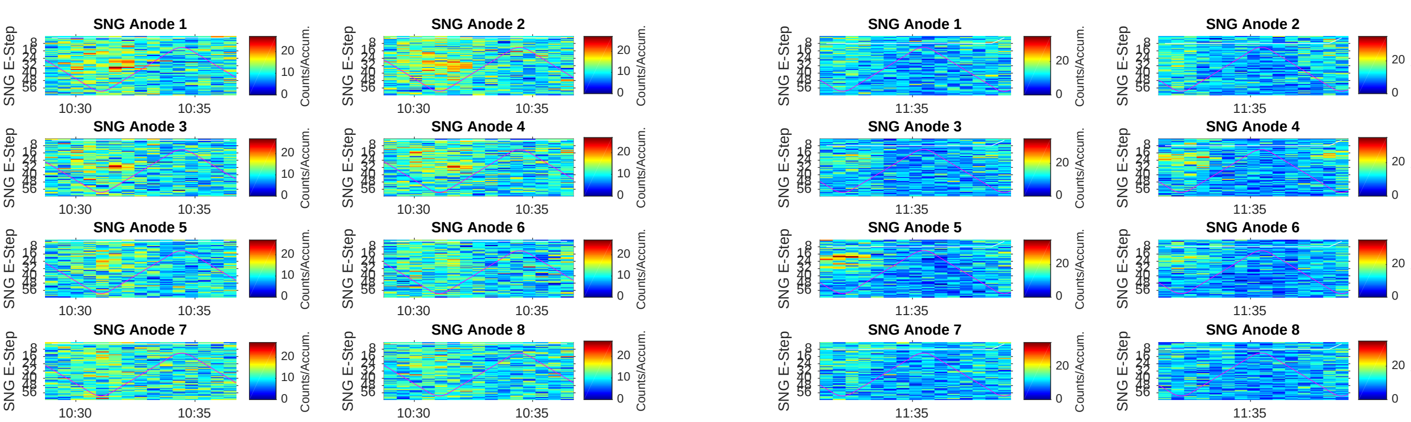

Figure 12. Two (left and right) low count intervals used in the LANL moments, all 8 anode shown for each.

4.5 Example TOF Case Where Ion Species Partitioning Fails

The main text describes how TOF can be less sensitive to W^+ ions than light ions, figure 13 is an example of that. It covers 5 back-to-back B-cycles (TOF records) in a high telemetry mode, near 20 R_S on the equator. The top panel shows the usual SNG spectrogram, with the magenta line indicating actuator angle and the white line the telemetry mode (=16). Two ion species are clearly visible, with W^+ counts dominating over those of H^+, but only have a significant presence in 3 of the 6 half actuation intervals. The second panel shows the TOF data (see the CAPS Users Guide for details), summed over the 5 B-cycles that correspond to the interval of the top panel. A red box indicates the area of the plot where light ions are found, and the blue box shows the equivalent (larger) water group ions area. As water ions pass through the start foil, they may break up to give an O^- ion or a neutral water group molecule; a count in either area is a sign that a water ion entered the instrument.

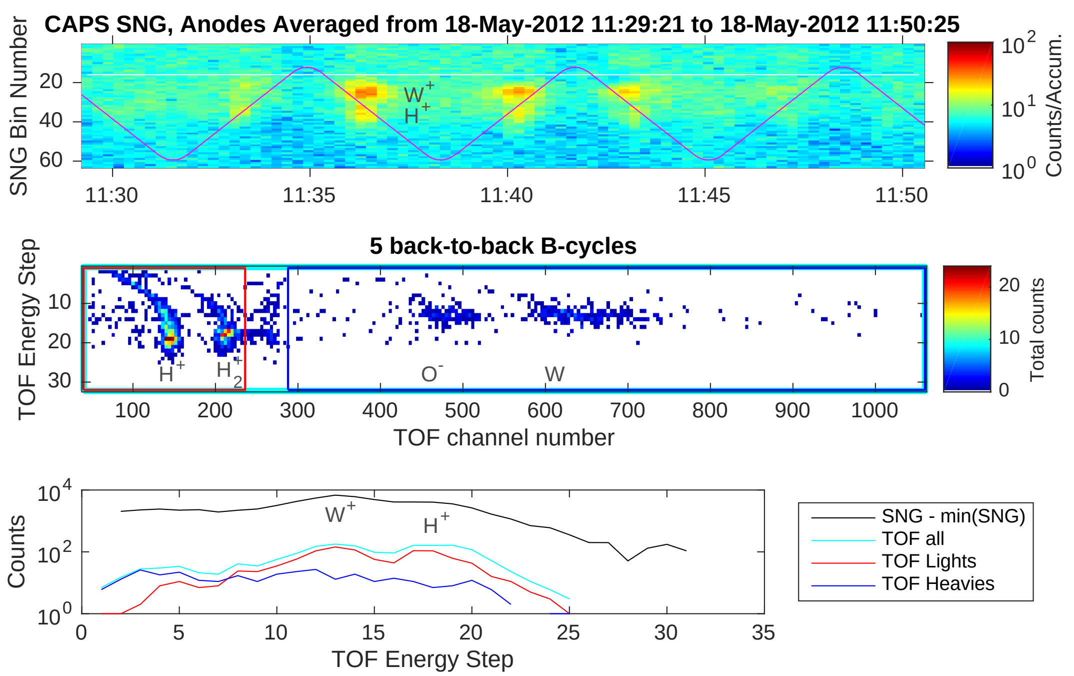

Figure 13. TOF composition vs. SNG. Top panel is SNG data, middle panel the corresponding TOF data and the lower panel shows the ion species partitioning.

It is clear from the figure that the SNG data observes a lot of W^+ when the actuator sweeps through the sub-corotating flow, while the TOF has a higher intensity of H^+, although this may be partly due to the water group area being wider and thus spreading out the counts. TOF data is susceptible to so-called ‘ghost peaks’, which can appear at all TOF channels (x-axis), but are usually only see of the dominant ion. The W^+ ions peak at around TOF energy step 13, and can be seen as a horizontal intermittent line of ghost counts in the red box at those energies.

The bottom panel collapses the data over time, and sums SNG energy steps (1-63) to match those of the TOF dataset (1-32). The black line shows the collapsed SNG data, with a high background but two ion species peaks visible with that of W^+ greater than the H^+. The cyan line shows the collapsed TOF data, with little background (as it is a coincidence measurement); still with two peaks present, but now they are of similar height, suggesting that TOF is less sensitive to W^+ ions. It is immediately obvious that there are far fewer total counts in the TOF than the SNG dataset. We may now sum up the counts at each energy step in the red and blue boxes of the middle panel, which are shown as the red and blue lines, the sum of which will be below the cyan line (as there is a region around 250-300 TOF channels that is excluded). What appears is that the water group ions in TOF are largely featureless with very low counts and the proton peak dominates, while also containing two roughly equal peaks - the extra peak around energy step 13 being due to the water ions ghost peaks.

Fitting such red or blue box TOF data would suggest the water group proportion of SNG counts is much lower than it actually is. In addition, the ghost peak of those water group ions have caused a secondary peak in the proton distribution that would skew any moments calculations.

The TOF fitting code used by LANL does remove a background from each energy step, so in high count regions for TOF these ghost peaks would be removed as a continuous background. However, when low count statistics areas such as these intermittent ones are encountered, there may not be enough ghost peaks at all TOF channels to be identified as a consistent background. This could allow W^+ ghost peaks to be interpreted as extra H^+ and H_2^+ ions, rather than being excluded, resulting in the code over-estimating the percentage of light ions and under-estimating those of water group.

The extent to which these issues occur, and how rarified water group densities in TOF records have to be before they are below the instrument's sensitivity are unknown and encouraged for future study.

5 Tables

5.1 The Binned LASP Dataset

Tables 1, 2 and 3 list the binned data used for the figures in this paper; a table each for the 50^{th} (medians), 25^{th} and 75^{th} percentiles respectively (separate tables to make a copy/paste easy). The velocity components are in the Saturn deSpun Sun system (see section 2 of this document).

Table 1. The medians of the binned LASP dataset of all magnetosphere data within 10° latitude of equator. (25^{th} and 75^{th} percentile provided in tables 2 and 3.)

Range R (R_S)	V_r (km/s)	V_θ (km/s)	V_ϕ (km/s)	$W^+ n$ (cm^{-3})	$W^+ T_\perp$ (eV)	$W^+ T_\parallel$ (eV)	$H^+ n$ (cm^{-3})	$H^+ T_\perp$ (eV)	$H^+ T_\parallel$ (eV)	Samples in bin
$05.5 \leq R < 06.0$	1.573	-0.036	44.887	25.436	92.870	34.358	4.116	11.890	8.882	759
$06.0 \leq R < 06.5$	0.343	0.093	47.406	21.352	104.986	43.310	3.418	12.266	8.305	682
$06.5 \leq R < 07.0$	0.841	-0.216	49.409	15.050	105.208	50.928	2.636	12.783	8.386	616
$07.0 \leq R < 07.5$	0.931	-0.521	52.893	10.771	122.544	70.149	1.969	17.867	10.410	525
$07.5 \leq R < 08.0$	0.874	-0.196	55.926	8.099	144.370	87.377	1.524	21.644	12.264	477
$08.0 \leq R < 08.5$	0.725	0.024	57.988	4.951	157.798	102.169	1.042	23.726	13.770	507
$08.5 \leq R < 09.0$	1.586	0.252	61.322	3.716	166.916	102.454	0.831	24.425	14.388	566
$09.0 \leq R < 09.5$	0.323	0.441	63.434	2.697	165.927	111.604	0.644	27.288	15.899	562
$09.5 \leq R < 10.0$	1.261	-0.213	65.285	2.129	165.010	122.245	0.527	25.008	14.430	410
$10.0 \leq R < 10.5$	0.500	-0.230	67.228	1.672	155.858	132.410	0.474	25.376	15.527	337
$10.5 \leq R < 11.0$	3.449	0.082	69.541	1.433	150.587	129.476	0.446	24.045	14.867	271
$11.0 \leq R < 11.5$	3.549	-1.149	70.460	1.221	146.236	124.538	0.362	23.871	14.273	267
$11.5 \leq R < 12.0$	4.450	-1.290	71.444	0.815	159.584	140.468	0.262	25.708	15.106	268
$12.0 \leq R < 12.5$	1.734	-2.301	73.078	0.604	166.941	160.820	0.227	30.432	17.152	236
$12.5 \leq R < 13.0$	4.467	-1.289	78.125	0.575	151.664	145.735	0.203	25.557	18.068	271
$13.0 \leq R < 13.5$	5.836	-0.333	81.274	0.550	161.012	147.863	0.205	26.798	17.259	237
$13.5 \leq R < 14.0$	2.599	-1.939	85.278	0.449	173.135	197.672	0.178	29.707	24.805	261
$14.0 \leq R < 14.5$	7.421	-1.158	89.074	0.305	218.017	220.555	0.156	33.134	29.011	215
$14.5 \leq R < 15.0$	7.152	-3.626	94.387	0.287	240.002	232.269	0.149	38.673	28.584	174
$15.0 \leq R < 15.5$	6.661	-4.563	92.728	0.252	206.541	226.455	0.136	35.815	29.777	129
$15.5 \leq R < 16.0$	-8.392	1.364	98.220	0.224	233.167	243.471	0.115	39.646	38.320	105
$16.0 \leq R < 16.5$	-3.430	-4.032	90.862	0.239	202.903	237.182	0.141	36.973	29.606	109
$16.5 \leq R < 17.0$	-3.696	-1.835	95.583	0.223	182.485	211.511	0.109	38.141	36.921	123
$17.0 \leq R < 17.5$	0.345	-3.282	91.097	0.224	177.838	229.245	0.134	31.932	26.535	128
$17.5 \leq R < 18.0$	6.420	-0.996	98.642	0.145	316.452	327.115	0.106	44.534	35.180	89
$18.0 \leq R < 18.5$	2.810	-5.299	96.294	0.180	244.223	257.621	0.088	42.000	35.178	93
$18.5 \leq R < 19.0$	16.273	3.115	113.352	0.140	404.649	365.424	0.084	62.699	45.666	146
$19.0 \leq R < 19.5$	10.663	1.607	128.253	0.102	465.255	418.393	0.080	77.944	56.102	126
$19.5 \leq R < 20.0$	1.890	-1.676	110.033	0.119	329.809	357.571	0.074	52.712	39.488	236
$20.0 \leq R < 20.5$	20.504	-6.670	120.331	0.099	423.744	371.759	0.077	67.260	54.380	108
$20.5 \leq R < 21.0$	20.126	2.068	104.907	0.129	360.163	362.587	0.094	60.341	46.735	121
$21.0 \leq R < 21.5$	25.189	-6.218	106.921	0.132	377.434	398.012	0.099	52.160	42.764	40
$21.5 \leq R < 22.0$	28.399	-1.164	116.498	0.107	303.054	288.575	0.073	66.588	50.640	57
$22.0 \leq R < 22.5$	30.903	-11.281	122.879	0.101	305.806	328.202	0.072	64.811	48.145	40
$22.5 \leq R < 23.0$	19.291	-4.865	114.255	0.107	230.115	243.933	0.069	65.989	51.258	54
$23.0 \leq R < 23.5$	18.721	-8.332	74.216	0.201	426.900	308.630	0.505	120.034	132.435	57
$23.5 \leq R < 24.0$	22.401	15.965	61.468	0.240	396.263	405.665	0.430	120.048	86.779	38
$24.0 \leq R < 24.5$	15.675	-1.725	75.941	0.171	497.182	417.671	0.311	121.916	87.988	54
$24.5 \leq R < 25.0$	20.865	-2.203	70.026	0.173	368.013	302.558	0.135	105.206	95.337	24
$25.0 \leq R < 25.5$	25.485	2.420	109.451	0.138	408.555	301.376	0.186	104.595	116.657	24
$25.5 \leq R < 26.0$	45.553	-1.397	66.252	0.155	322.721	322.765	0.151	114.940	50.649	20
$26.0 \leq R < 26.5$	43.874	-10.120	120.872	0.105	310.725	312.793	0.053	76.583	60.951	41
$26.5 \leq R < 27.0$	53.469	4.263	109.933	0.089	323.423	321.554	0.056	65.614	52.649	24
$27.0 \leq R < 27.5$	39.926	9.397	132.007	0.070	408.048	336.802	0.075	92.744	80.100	14
$27.5 \leq R < 28.0$	61.921	-5.317	106.451	0.080	284.677	249.414	0.061	50.716	30.127	17
$28.0 \leq R < 28.5$	79.605	-20.349	193.575	0.053	727.983	540.758	0.041	178.617	155.612	8
$28.5 \leq R < 29.0$	33.047	-0.949	72.591	0.137	599.927	392.979	0.242	125.141	92.593	27
$29.0 \leq R < 29.5$	25.193	1.210	86.102	0.136	272.733	253.054	0.167	110.934	53.618	24
$29.5 \leq R < 30.0$	44.725	-4.116	132.757	0.104	473.041	365.308	0.071	109.514	106.530	19

Table 2. The 25^{th} percentile of the binned LASP dataset of all magnetosphere data within 10° latitude of equator. (Medians and 75^{th} percentile provided in tables 1 and 3.)

Range R (R_S)	V_r (km/s)	V_θ (km/s)	V_ϕ (km/s)	$W^+\ n$ (cm^{-3})	$W^+\ T_\perp$ (eV)	$W^+\ T_\parallel$ (eV)	$H^+\ n$ (cm^{-3})	$H^+\ T_\perp$ (eV)	$H^+\ T_\parallel$ (eV)	Samples in bin
$05.5 \le R < 06.0$	-1.239	-1.650	41.575	18.577	68.103	26.056	3.619	9.627	6.992	759
$06.0 \le R < 06.5$	-2.284	-1.586	44.868	16.534	85.714	31.719	2.865	9.413	6.573	682
$06.5 \le R < 07.0$	-3.497	-1.815	47.153	11.637	83.438	36.947	2.179	9.052	6.634	616
$07.0 \le R < 07.5$	-3.216	-2.265	50.187	6.992	94.442	50.112	1.451	10.744	7.302	525
$07.5 \le R < 08.0$	-2.635	-1.978	52.704	5.515	115.836	63.657	1.091	14.574	8.410	477
$08.0 \le R < 08.5$	-3.515	-2.268	55.383	3.016	126.136	74.713	0.678	16.892	9.360	507
$08.5 \le R < 09.0$	-2.627	-1.498	57.602	2.225	130.562	78.850	0.561	17.570	9.491	566
$09.0 \le R < 09.5$	-4.400	-1.623	59.247	1.777	135.876	86.456	0.427	20.195	10.362	562
$09.5 \le R < 10.0$	-3.743	-2.686	59.632	1.395	132.987	93.702	0.350	19.213	10.949	410
$10.0 \le R < 10.5$	-4.329	-3.284	61.345	1.025	132.675	107.546	0.344	19.608	11.131	337
$10.5 \le R < 11.0$	-0.889	-2.205	63.372	0.818	127.353	102.549	0.280	18.439	10.578	271
$11.0 \le R < 11.5$	-0.576	-3.792	65.031	0.757	122.783	95.462	0.256	17.729	9.834	267
$11.5 \le R < 12.0$	-3.598	-4.354	66.779	0.562	127.078	102.316	0.203	18.465	11.006	268
$12.0 \le R < 12.5$	-4.068	-6.264	67.066	0.467	130.354	121.983	0.173	20.216	12.736	236
$12.5 \le R < 13.0$	-6.770	-7.214	70.609	0.410	124.549	110.934	0.151	20.392	12.424	271
$13.0 \le R < 13.5$	-3.706	-4.550	72.387	0.374	118.249	118.729	0.155	19.811	12.475	237
$13.5 \le R < 14.0$	-7.893	-6.064	75.410	0.314	123.039	132.850	0.134	20.379	14.630	261
$14.0 \le R < 14.5$	-2.110	-6.131	80.870	0.232	151.516	155.047	0.119	22.445	17.037	215
$14.5 \le R < 15.0$	-0.238	-8.540	84.748	0.188	168.041	163.837	0.107	26.050	19.359	174
$15.0 \le R < 15.5$	-6.113	-9.303	80.776	0.190	165.698	159.340	0.102	28.166	20.442	129
$15.5 \le R < 16.0$	-17.595	-5.831	82.038	0.162	140.786	149.586	0.076	22.940	22.447	105
$16.0 \le R < 16.5$	-18.758	-8.950	82.294	0.165	135.423	160.545	0.101	25.177	19.360	109
$16.5 \le R < 17.0$	-21.564	-5.749	82.892	0.157	119.471	161.307	0.083	20.882	19.298	123
$17.0 \le R < 17.5$	-11.158	-6.784	83.064	0.157	140.176	158.504	0.097	21.206	17.591	128
$17.5 \le R < 18.0$	-14.751	-9.386	85.619	0.109	160.937	194.072	0.079	27.768	25.549	89
$18.0 \le R < 18.5$	-14.816	-11.713	88.366	0.123	163.948	181.955	0.068	32.140	25.869	93
$18.5 \le R < 19.0$	-4.126	-7.697	92.420	0.093	237.459	263.818	0.068	38.487	31.963	146
$19.0 \le R < 19.5$	-13.374	-8.568	108.696	0.074	270.671	269.680	0.062	48.725	37.220	126
$19.5 \le R < 20.0$	-9.518	-10.673	90.698	0.089	202.598	224.479	0.058	34.661	27.258	236
$20.0 \le R < 20.5$	3.602	-16.177	97.910	0.073	227.957	214.560	0.060	41.553	32.865	108
$20.5 \le R < 21.0$	7.245	-12.680	92.203	0.088	223.778	259.624	0.073	37.408	32.449	121
$21.0 \le R < 21.5$	17.460	-11.378	98.441	0.110	198.017	256.532	0.060	40.824	30.885	40
$21.5 \le R < 22.0$	3.826	-8.888	98.019	0.076	171.670	184.906	0.056	36.498	28.774	57
$22.0 \le R < 22.5$	9.038	-18.478	104.082	0.069	181.029	206.330	0.051	38.895	29.148	40
$22.5 \le R < 23.0$	10.534	-18.469	96.796	0.072	160.481	145.110	0.051	41.272	37.666	54
$23.0 \le R < 23.5$	-1.121	-30.787	66.014	0.131	344.956	254.304	0.360	87.381	90.983	57
$23.5 \le R < 24.0$	15.306	5.637	57.020	0.172	350.391	366.265	0.292	99.700	72.720	38
$24.0 \le R < 24.5$	10.978	-20.260	67.114	0.070	425.682	346.626	0.084	103.663	76.524	54
$24.5 \le R < 25.0$	10.523	-30.308	50.106	0.081	128.721	152.292	0.085	34.177	23.767	24
$25.0 \le R < 25.5$	16.525	-32.239	61.005	0.070	363.318	247.659	0.077	87.492	64.004	24
$25.5 \le R < 26.0$	26.047	-16.551	56.216	0.108	251.589	235.784	0.060	70.624	32.501	20
$26.0 \le R < 26.5$	24.524	-19.580	79.459	0.082	182.441	191.387	0.041	37.091	35.139	41
$26.5 \le R < 27.0$	26.651	-14.663	72.958	0.055	238.764	216.012	0.043	46.718	44.870	24
$27.0 \le R < 27.5$	33.280	-6.382	71.167	0.049	198.490	239.458	0.047	39.971	44.919	14
$27.5 \le R < 28.0$	43.294	-23.161	86.152	0.067	141.940	141.960	0.044	31.937	16.982	17
$28.0 \le R < 28.5$	67.930	-25.209	153.619	0.038	548.121	389.832	0.031	101.398	72.736	8
$28.5 \le R < 29.0$	24.465	-4.221	62.322	0.097	443.826	354.049	0.117	112.182	74.463	27
$29.0 \le R < 29.5$	18.634	-8.648	74.029	0.083	217.723	191.100	0.071	48.251	30.904	24
$29.5 \le R < 30.0$	31.356	-24.104	92.762	0.063	334.912	174.526	0.055	78.795	62.151	19

Table 3. The 75^{th} percentile of the binned LASP dataset of all magnetosphere data within 10° latitude of equator. (Medians and 25^{th} percentile provided in tables 1 and 2.)

Range R (R_S)	V_r (km/s)	V_θ (km/s)	V_ϕ (km/s)	$W^+ n$ (cm^{-3})	$W^+ T_\perp$ (eV)	$W^+ T_\parallel$ (eV)	$H^+ n$ (cm^{-3})	$H^+ T_\perp$ (eV)	$H^+ T_\parallel$ (eV)	Samples in bin
$05.5 \le R < 06.0$	5.647	2.158	48.007	30.963	114.470	52.492	4.851	14.842	10.950	759
$06.0 \le R < 06.5$	3.912	1.251	50.034	24.633	134.519	67.810	3.969	17.263	11.420	682
$06.5 \le R < 07.0$	3.792	1.361	52.446	18.926	152.316	85.947	3.305	20.157	12.063	616
$07.0 \le R < 07.5$	4.310	1.150	56.212	14.384	169.694	104.662	2.736	25.558	14.520	525
$07.5 \le R < 08.0$	3.568	1.410	59.793	10.000	192.975	127.289	2.123	28.215	18.236	477
$08.0 \le R < 08.5$	3.843	2.001	63.456	6.939	194.684	133.575	1.582	34.561	20.965	507
$08.5 \le R < 09.0$	6.210	3.069	65.176	5.055	204.141	139.378	1.104	37.635	22.987	566
$09.0 \le R < 09.5$	4.611	2.674	67.005	3.890	208.049	148.850	0.909	40.773	24.605	562
$09.5 \le R < 10.0$	5.533	2.368	68.866	3.075	217.359	163.354	0.737	39.690	24.342	410
$10.0 \le R < 10.5$	6.303	3.070	71.003	2.306	203.012	203.640	0.624	41.120	23.526	337
$10.5 \le R < 11.0$	10.037	4.120	76.461	1.940	211.874	204.898	0.604	34.865	23.697	271
$11.0 \le R < 11.5$	10.245	1.903	77.217	1.733	224.643	214.919	0.497	37.414	22.730	267
$11.5 \le R < 12.0$	12.253	1.770	77.031	1.204	211.444	209.882	0.356	35.154	25.172	268
$12.0 \le R < 12.5$	11.858	2.842	79.612	0.807	253.633	248.720	0.272	44.752	35.384	236
$12.5 \le R < 13.0$	12.638	1.770	84.600	0.795	216.454	232.685	0.275	38.489	30.633	271
$13.0 \le R < 13.5$	11.997	3.279	88.132	0.824	236.535	236.315	0.295	37.139	27.854	237
$13.5 \le R < 14.0$	13.509	1.198	94.535	0.636	264.023	306.765	0.245	44.569	40.790	261
$14.0 \le R < 14.5$	15.877	4.081	100.232	0.484	345.555	349.033	0.197	60.978	41.688	215
$14.5 \le R < 15.0$	18.217	0.406	104.386	0.397	367.484	329.343	0.190	59.876	46.417	174
$15.0 \le R < 15.5$	19.102	0.450	103.712	0.372	319.110	336.967	0.174	53.334	54.960	129
$15.5 \le R < 16.0$	12.504	5.415	113.882	0.345	377.527	348.939	0.169	60.668	63.209	105
$16.0 \le R < 16.5$	11.928	0.501	104.285	0.352	379.112	417.007	0.197	59.292	53.841	109
$16.5 \le R < 17.0$	10.080	3.094	111.573	0.300	334.022	367.205	0.153	65.703	63.202	123
$17.0 \le R < 17.5$	14.032	1.160	102.874	0.305	280.625	296.683	0.161	57.005	39.779	128
$17.5 \le R < 18.0$	26.758	9.054	111.514	0.213	473.532	556.274	0.149	68.111	57.668	89
$18.0 \le R < 18.5$	17.302	2.704	113.941	0.260	445.348	427.425	0.125	68.206	54.292	93
$18.5 \le R < 19.0$	33.212	10.959	132.957	0.206	737.687	592.237	0.115	103.036	81.821	146
$19.0 \le R < 19.5$	37.501	16.801	150.850	0.133	948.317	706.796	0.101	129.303	90.477	126
$19.5 \le R < 20.0$	32.325	10.382	136.844	0.181	537.481	460.038	0.111	88.631	62.308	236
$20.0 \le R < 20.5$	36.435	4.204	147.877	0.164	622.553	615.168	0.094	96.688	73.091	108
$20.5 \le R < 21.0$	37.698	10.225	135.173	0.182	505.635	544.183	0.142	113.786	74.406	121
$21.0 \le R < 21.5$	39.317	-0.753	119.756	0.175	452.442	513.143	0.133	58.648	59.109	40
$21.5 \le R < 22.0$	53.403	5.107	141.483	0.169	620.003	676.455	0.111	110.047	70.758	57
$22.0 \le R < 22.5$	45.511	-2.269	134.459	0.180	476.580	552.027	0.104	134.189	94.799	40
$22.5 \le R < 23.0$	32.909	2.590	134.675	0.160	522.666	378.778	0.104	99.094	67.807	54
$23.0 \le R < 23.5$	49.691	2.631	93.180	0.266	833.622	370.673	0.552	151.272	166.107	57
$23.5 \le R < 24.0$	26.926	20.614	73.753	0.287	432.170	474.231	0.506	137.253	109.058	38
$24.0 \le R < 24.5$	22.650	20.347	127.918	0.206	679.641	578.849	0.388	144.861	158.980	54
$24.5 \le R < 25.0$	40.834	14.380	107.411	0.196	420.150	496.177	0.363	121.368	147.560	24
$25.0 \le R < 25.5$	81.251	10.809	136.240	0.241	656.313	460.540	0.545	137.031	154.036	24
$25.5 \le R < 26.0$	50.558	6.075	126.417	0.202	455.098	483.047	0.180	183.174	106.295	20
$26.0 \le R < 26.5$	56.466	0.607	137.021	0.126	466.207	408.077	0.138	131.138	81.946	41
$26.5 \le R < 27.0$	66.256	17.041	141.837	0.114	439.085	481.659	0.182	123.513	80.068	24
$27.0 \le R < 27.5$	65.436	33.046	184.759	0.146	964.490	721.039	0.109	131.417	115.933	14
$27.5 \le R < 28.0$	74.418	8.487	154.920	0.109	356.238	360.296	0.082	86.262	46.797	17
$28.0 \le R < 28.5$	117.614	-3.624	203.357	0.092	806.728	642.201	0.069	244.320	256.462	8
$28.5 \le R < 29.0$	54.523	2.920	81.630	0.152	663.405	452.482	0.255	135.787	119.451	27
$29.0 \le R < 29.5$	48.615	10.393	102.036	0.191	507.480	365.432	0.244	140.490	99.809	24
$29.5 \le R < 30.0$	57.310	6.025	159.081	0.156	550.332	407.837	0.248	120.749	175.930	19

5.2 Power Law Fits for LASP and Thomsen2010 Data

Table 4 shows the power law fits from Thomsen2010 (to the precision they provide) and from the LASP dataset when calculated in a similar way; equations are provided in the main text for these, except for H_2^+. The LASP $0.5R_S$ binned values (Tables 1, 2 and 3 above) are suggested for science use, instead of a power law, as they are more accurate representations.

Table 4. Power Law Fits to Density Profiles

L Dependence of $\|Lat\| < 5°$ Mean Densities in 1R_S L Bins (6 < L < 17): $n = CL^{-m}$					
Thomsen2010	Parameter	H^+	H_2^+	W^+	Total Ions
(a)	C (cm^{-3})	10.1×10^3	79.7	87.2×10^5	13.8×10^5
(a)	m	4.28	2.88	6.62	5.68
(a,b)	Corr. Coeff.	0.993	0.895	0.993	0.998

R Dependence of $\|Lat\| < 10°$ Median Densities (unweighted) in 0.5R_S Bins (6 < R_S < 17): $n = CR^{-m}$					
LASP	Parameter	H^+	H_2^+	W^+	Total Ions
	C (cm^{-3})	$(5.37\pm1.59)\times10^3$	-	$(2.05\pm0.67)\times10^5$	$(1.79\pm0.55)\times10^5$
	m	4.01 ± 0.15	-	5.00 ± 0.17	4.84 ± 0.16
(b)	Corr. Coeff.	0.998	-	0.999	0.999

a) Columns and values from Table 1 of Thomsen2010, not calculated from the PDS LANL moments.

b) Correlation coefficient is the R-value.

Other differences between the two methods are:

1. Thomsen2010 used mean bins, LASP used median bins, however Thomsen2010 state their mean and median values were similar in this range.
2. Thomsen2010 study radial fits includes data to 5° off the equator, LASP to 10°.
3. Thomsen2010 study had the first 4.5 years of Saturnian CAPS data, LASP has all 9 years.
4. Thomsen2010 had bins 1 R_S wide, while LASP has bins 0.5 R_S wide.
5. Thomsen2010 used the (lower) scalar SNG efficiency, whereas LASP used the (higher) energy dependent SNG efficiencies.
6. Thomsen2010 worked in L-Shell, but at these latitudes $1L \simeq 1R_S$.

6 Data Set S1: The LASP Forward Model Fit Parameters (Both Good and Bad)

The dataset of fitted parameters used in this study is included in the supplementary material as a comma separated variable (csv) file named "2017JA024117-ds01.csv". It contains all the fits and calculated uncertainties, even the unphysical ones, so it is recommended that you only use the records that were used for analysis in this paper; identified by the csv file having a 'used in paper' column named JGR [1 = used in paper (passed post-pruning), 0 = not used in paper (failed post-pruning)]. Even then we recommend to use trends in the data rather than absolute values as not all records are great fits, and it is certain that some bad fits still managed to pass our post-pruning tests.

The file has Windows line endings (\r\n) and the first line is a header row, with columns described in table 6. The 9 fitted parameters (with uncertainties) are provided in Table 5:

Paramter				Column names in CSV file		
V_r	$\pm$	σ_{V_r}	$\Rightarrow$	Fit_Vr	$\pm$	Sigma_Vr
V_θ	$\pm$	σ_{V_θ}	$\Rightarrow$	Fit_Vt	$\pm$	Sigma_Vt
V_ϕ	$\pm$	σ_{V_ϕ}	$\Rightarrow$	Fit_Vp	$\pm$	Sigma_Vp
n_{W+}	$\pm$	$\sigma_{n_{W+}}$	$\Rightarrow$	Fit_Wn	$\pm$	Sigma_Wn
$T_{\perp W+}$	$\pm$	$\sigma_{T_{\perp W+}}$	$\Rightarrow$	Fit_WTperp	$\pm$	Sigma_WTperp
$T_{\parallel W+}$	$\pm$	$\sigma_{T_{\parallel W+}}$	$\Rightarrow$	Fit_WTpara	$\pm$	Sigma_WTpara
n_{H+}	$\pm$	$\sigma_{n_{H+}}$	$\Rightarrow$	Fit_Hn	$\pm$	Sigma_Hn
$T_{\perp H+}$	$\pm$	$\sigma_{T_{\perp H+}}$	$\Rightarrow$	Fit_HTperp	$\pm$	Sigma_HTperp
$T_{\parallel H+}$	$\pm$	$\sigma_{T_{\parallel H+}}$	$\Rightarrow$	Fit_HTpara	$\pm$	Sigma_HTpara

Table 5: Mapping fitted parameters to the CSV file columns.

The uncertainties ("Sigma_*") is the parameter uncertainty for each of the 9 free parameters, as found by taking the square root of the diagonal of the 9×9 covariance matrix for the fitted interval.

If all the free parameters are assumed to be independent (*but they are definitely not independent*), then the independent standard deviation of each fit may be calculated, which are the "Ind_SDev_*" values; found by taking the square root of the variance of each parameter fit. These are for reference only, we suggest you never use them and **always** use the Sigma_* values for your uncertainties.

Units for each parameter are listed in table 6, and the co-ordinate system for the velocities is SSS (see section 2).

Table 6 follows, split over two pages.

Column Name	**Description**	**Units**
UTC	Time	UTC
delta_t	Half the accumulation period, e.g. UTC $\pm$ delta_t	Seconds
SC_R	SpaceCraft Radial Distance	R_S
SC_LT	SpaceCraft Local Time	Hours
SC_LAT	SpaceCraft Latitude	Degrees
SC_COROT	Corotation speed at this location	km/s
LowerLim_Vr	Lower Limit for fitting procedure for V_r	km/s
LowerLim_Vt	Lower Limit for fitting procedure for V_θ	km/s
LowerLim_Vp	Lower Limit for fitting procedure for V_ϕ	km/s
LowerLim_Wn	Lower Limit for fitting procedure for W^+ density	cm^{-3}
LowerLim_WTperp	Lower Limit for fitting procedure for W^+ $T_\perp$	eV
LowerLim_WTpara	Lower Limit for fitting procedure for W^+ $T_\parallel$	eV
LowerLim_Hn	Lower Limit for fitting procedure for H^+ density	cm^{-3}
LowerLim_HTperp	Lower Limit for fitting procedure for H^+ $T_\perp$	eV
LowerLim_HTpara	Lower Limit for fitting procedure for H^+ $T_\parallel$	eV
UpperLim_Vr	Upper Limit for fitting procedure for V_r	km/s
UpperLim_Vt	Upper Limit for fitting procedure for V_θ	km/s
UpperLim_Vp	Upper Limit for fitting procedure for V_ϕ	km/s
UpperLim_Wn	Upper Limit for fitting procedure for W^+ density	cm^{-3}
UpperLim_WTperp	Upper Limit for fitting procedure for W^+ $T_\perp$	eV
UpperLim_WTpara	Upper Limit for fitting procedure for W^+ $T_\parallel$	eV
UpperLim_Hn	Upper Limit for fitting procedure for H^+ density	cm^{-3}
UpperLim_HTperp	Upper Limit for fitting procedure for H^+ $T_\perp$	eV
UpperLim_HTpara	Upper Limit for fitting procedure for H^+ $T_\parallel$	eV
Number_Data_Points	Number of data points used in the fit	#
Count_Min	Minimum counts/accumulation in fitted interval	Counts/Accum.
Count_Max	Maximum counts/accumulation in fitted interval	Counts/Accum.
Fit_Cost	Cost function (= χ_r^2 value + any Penalties)	Unitless
Fit_Vr	Best Fit value for V_r	km/s

Fit_Vt	Best Fit value for V_θ	km/s
Fit_Vp	Best Fit value for V_ϕ	km/s
Fit_Wn	Best Fit value for W^+ density	cm^{-3}
Fit_WTperp	Best Fit value for W^+ $T_\perp$	eV
Fit_WTpara	Best Fit value for W^+ $T_\parallel$	eV
Fit_Hn	Best Fit value for H^+ density	cm^{-3}
Fit_HTperp	Best Fit value for H^+ $T_\perp$	eV
Fit_HTpara	Best Fit value for H^+ $T_\parallel$	eV
Sigma_Vr	Uncertainty on Best Fit value for V_r	km/s
Sigma_Vt	Uncertainty on Best Fit value for V_θ	km/s
Sigma_Vp	Uncertainty on Best Fit value for V_ϕ	km/s
Sigma_Wn	Uncertainty on Best Fit value for W^+ density	cm^{-3}
Sigma_WTperp	Uncertainty on Best Fit value for W^+ $T_\perp$	eV
Sigma_WTpara	Uncertainty on Best Fit value for W^+ $T_\parallel$	eV
Sigma_Hn	Uncertainty on Best Fit value for H^+ density	cm^{-3}
Sigma_HTperp	Uncertainty on Best Fit value for H^+ $T_\perp$	eV
Sigma_HTpara	Uncertainty on Best Fit value for H^+ $T_\parallel$	eV
Ind_SDev_Vr	Standard Deviation on Best Fit value for V_r	km/s
Ind_SDev_Vt	Standard Deviation on Best Fit value for V_θ	km/s
Ind_SDev_Vp	Standard Deviation on Best Fit value for V_ϕ	km/s
Ind_SDev_Wn	Standard Deviation on Best Fit value for W^+ density	cm^{-3}
Ind_SDev_WTperp	Standard Deviation on Best Fit value for W^+ $T_\perp$	eV
Ind_SDev_WTpara	Standard Deviation on Best Fit value for W^+ $T_\parallel$	eV
Ind_SDev_Hn	Standard Deviation on Best Fit value for H^+ density	cm^{-3}
Ind_SDev_HTperp	Standard Deviation on Best Fit value for H^+ $T_\perp$	eV
Ind_SDev_HTpara	Standard Deviation on Best Fit value for H^+ $T_\parallel$	eV
[We STRONGLY recommend using Sigma_* values for error bars rather than Ind_*]		
JGR	1 = Record was used in paper (passed post-pruning)	Unitless
	0 = Record was not used in paper, as it was considered a bad fit (failed post-pruning)	

Table 6: Description of the columns in file 2017JA024117-ds01.csv